Methods for Modeling Vegetated Channels as Porous Media (OpenFOAM)

James Vincent Brice, MIT Department of Architecture

2.29 Numerical Fluid Mechanics | Spring 2022

INTRODUCTION

Traditionally, coastal adaptation has been implemented in the form of static, hard infrastructure like seawalls, dikes, and groins (Moosavi, 2017). Although successful in stabilizing coastlines and preventing flooding due to storm-surge, these structures are the cause of several negative externalities, often destroying tidal regimes (squeezing) (Torio & Chmura, 2013), increasing seaward erosion (scouring) (Sutherland, Obhrai, Whitehouse, & Pearce, 2007), and closing off estuarine habitats critical to the development of marine organisms (Munsch, Cordell, Toft, & Morgan, 2014).

Conversely, increased understanding of the hydrodynamic and ecological co-benefits coastal habitats, vegetation, and reefs provide has driven efforts to explore the efficacy of their implementation in coastal adaptation projects. When naturally occurring, these habitats are a rich source of ecosystem services globally and can be considered some of the most valuable on Earth (Barbier, et al., 2011), but increased human development of the shoreline and anthropogenic effects of climate change have led to their degradation and decreased functionality. “Nature-based solutions” (NBS) for coastal adaptation seek to capitalize on the services these ecosystems provide by designing landscapes that mimic their wild capacity, often through a combination of ecological restoration, landscape architecture, and coastal engineering.

Despite this, many coastal scale flood models are unable to capture the hydrodynamics of vegetated fields (“bathtub models”), and those that can have only been implemented in a few test cases (Hu, Chen, & Wang, 2015). There’s a great deal of research that still needs to be done regarding these numerical flood models and how their usage informs urban waterfront adaptation and design. Its with this in mind that I’ve chosen to explore methods for modeling vegetated channels in the open-source CFD solver OpenFOAM.

MATHEMATICAL MODELS

There have been many approaches to modeling wave damping by vegetation, typically through a combination of semi-analytical methods and empirical techniques. A direct force calculation approach involves solving the Morison Equation given here

$$F = F_D + F_I = \frac{1}{2}\rho C_D d h_{pw} U_w |U_w| + \frac{1}{4}\rho C_M \pi h_{pw} d^2 \frac{\partial U_w}{\partial t}$$

where F_D is the drag force and F_I is the inertial force. Since the inertial term acts out of phase with the velocity (Mendez & Losada, 2004), the drag coefficient , C_D , is understood to be the primary driver in wave damping.

Several numerical models have been developed to investigate wave-vegetation interactions, usually by solving the Reynolds-Averaged Navier-Stokes Equations (RANS) with an added sink term to model the resistance generated by the vegetated field (Li & and Yan, 2007). Others have implemented the Boussinesq or shallow-water wave equations (Augustin, Irish, & and Lynett, 2009) (Wu & Marsooli, 2012).

Still others have explored an alternative approach, choosing to model vegetated fields as porous media (Hadadpour, Paul, & Oumeraci, 2019) (Zinke, 2012). These methods are unique in that they solve a volume-averaged set of governing equations, where flow resistance is determined by a pore Reynolds number based on the mean

pore velocity and the mean void nearest neighbor distance between individual vegetation. Although porous media is typically characterized primarily by the ratio between the total volume and the pore space, this definition may not fully capture the dynamics in a vegetated system which often has a very high porosity (upwards of 0.9). (Hadadpour, Paul, & Oumeraci, 2019) redefined porosity in terms known plant canopy parameters, namely the leaf area index (LAI) which describes both leaf length and shoot density. It's with this method that I have explored implementation in OpenFOAM.

NUMERICAL METHODS

Governing Equations

The *'porousWaveFoam'* solver uses the volume-averaged Reynolds-averaged Navier-Stokes (VARANS) equations discretized with a finite volume formulation on a collocated grid (Jensen, Jacobsen, & Christensen, 2014). The equations are derived to compute fluid flow within the porous media zone without resolving the entire complexity of the pore geometry, greatly reducing computational cost.

Starting from the incompressible RANS equations as given by the ensemble averaging process described in (Ferziger, Perić, & & Street, 2002), we have

$$\frac{\partial \rho \overline{u_i}}{\partial t} + \frac{\partial \rho \overline{u_j u_i}}{\partial x_i} = -\frac{\partial p}{\partial x_i} + g_i x_j \frac{\partial \rho}{\partial x_i} + \frac{\partial}{\partial x_j}\mu\left(\frac{\partial \overline{u_i}}{\partial x_j} + \frac{\partial \overline{u_j}}{\partial x_i}\right)$$

$$\frac{\partial \overline{u_i}}{\partial x_i} = 0$$

which are then volume averaged over a length scale, r_0, defined relative to the pore length scale and macroscopic length scale as in Figure 1. Definition of volume averages and length scales (Jensen et al., 2014) using the volume-averaging operator

$$\left\langle \frac{\partial \overline{u_i}}{\partial x_i} \right\rangle = \frac{\partial \langle \overline{u_i} \rangle}{\partial x_i} + \frac{1}{V}\int_S \overline{u_i} \cdot \hat{n} dA$$

and the following velocity decomposition

$$\overline{u_i} = \langle \overline{u_i} \rangle + \overline{u_i}''$$

which gives

$$(1 + C_m)\frac{\partial}{\partial t}\frac{\rho \langle \overline{u_i} \rangle}{n} + \frac{1}{n}\frac{\partial}{\partial x_i}\frac{\rho \langle \overline{u_j} \rangle \langle \overline{u_i} \rangle}{n} + \frac{1}{n}\frac{\partial \rho \left\langle \overline{u_i' u_j'} \right\rangle}{\partial x_j}$$
$$= -\frac{\partial \langle \overline{p} \rangle^f}{\partial x_i} + g_i x_j \frac{\partial \rho}{\partial x_i}$$
$$+ \frac{1}{n}\frac{\partial}{\partial x_j}\mu\left(\frac{\partial \langle \overline{u_i} \rangle}{\partial x_j} + \frac{\partial \langle \overline{u_j} \rangle}{\partial x_i}\right) + F_i$$

$$\frac{\partial \langle \overline{u_i} \rangle}{\partial x_i} = 0$$

where the inclusion of F_i is due to the appearance of terms in the momentum equation as a result of the volume-averaging procedure that cannot be solved without a closure model. Here the Darcy-Forcheimer equation is applied to model the porous resistance terms, defined as

$$F_i = a\rho \langle \overline{u_i} \rangle + b\sqrt{\langle \overline{u_j} \rangle \langle \overline{u_i} \rangle}\langle \overline{u_i} \rangle$$

where a and b are the resistance coefficients given by (Van Gent, 1995)

$$a = \alpha \frac{(1-n)^2}{n^3}\frac{\mu}{\rho d_{50}^2}$$

$$b = \beta\left(1 + \frac{7.5}{KC}\right)\frac{1-n}{n^3}\frac{1}{d_{50}}$$

And α and β are empirically defined.

Additionally, it's argued that the third term on the left-hand side of volume-averaged momentum equation (which describes the turbulent fluctuations and typically requires its own closure model) is captured within the empirically determined resistance coefficients *a* and *b*, and is therefore included in the resistance term F_i as well.

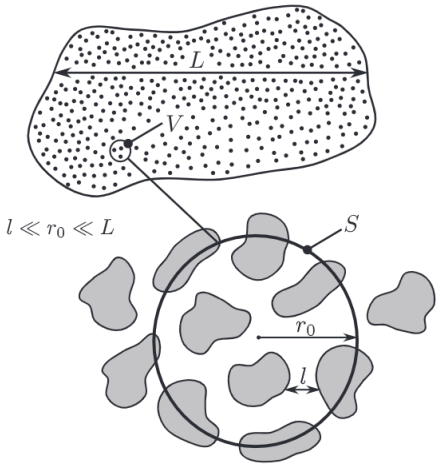

Figure 1. Definition of volume averages and length scales (Jensen et al., 2014)

Free-Surface Tracking

The *'waves2Foam'* package extends the free-surface tracking method employed in the native OpenFOAM code to wave generation, namely via the Volume-of-Fluid (VOF) method. In this method, the Navier-Stokes equations are solved for two fluids simultaneously on a single domain and tracked by a scalar field, γ. γ gives 1 for the fluid phase, 0 for the gas phase, and an intermediate value at the free surface which represents the ratio between the amount of gas and the amount of liquid present within a single computational cell. This scalar field is calculated with the advection equation

$$\frac{\partial \gamma}{\partial t} + \frac{1}{n}\frac{\partial}{\partial x_i}\left(\langle \overline{u_i}^r \rangle \gamma(1-\gamma)\right) = 0$$

also known as the volume-fraction equation. Given the sharp boundary between the liquid and the gas phase at the free surface, γ is discontinuous and susceptible to instability (Jacobsen, Fuhrman, & Fredsøe, 2012). The chosen numerical scheme must be sensitive to this and often requires smoothing (the last term on the left-hand side is a compression term designed to minimize this). In OpenFOAM, an explicit first-order time integration scheme is employed with a flux limiter on the divergence term to achieve the required stability condition (Jacobsen, Fuhrman, & Fredsøe, 2012).

Boundary Conditions

To accurately model waves within the numerical wave flume, boundary conditions need to be set in order to reduce wave reflection at the boundary. Two types of approaches are typically used: those that allow the wave to radiate out (Sommerfeld wave equation) and those that dampen the waves in a modified zone just before the boundary. The latter in employed in this algorithm and is called a relaxation zone or active sponge layer. Often defined at both the inlet and the outlet of the computational domain, these relaxation zones reduce wave reflection at the boundaries, eliminating contamination within the domain (in the case of reflection from the outlet boundary) and internal reflection at the inlet boundary which interferes with the wave maker and has been shown to lead to divergent solutions (Jacobsen, Fuhrman, & Fredsøe, 2012).

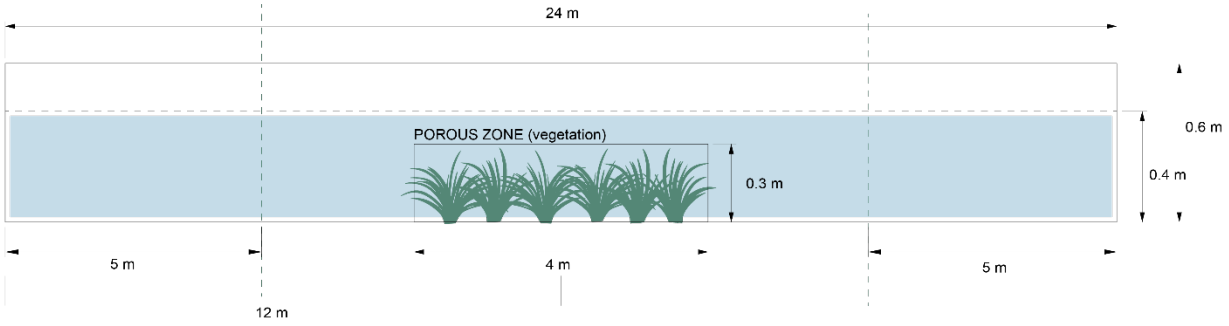

Figure 2. Diagram detailing the computational domain for the present test case, based of physical experiments conducted in the Nepf Lab and described in (Zhang et al. 2014)

The relaxation zones work by starting with an analytical solution to the wave (given by the chosen wave theory) and then applying a weighting function

$$\chi(\xi) = 1 - \frac{exp(\xi^{\beta} - 1)}{exp(1) - 1)}$$

where ξ is a local coordinate in the relaxation zone valued from 1 at the inlet to 0 at the interface with the computational domain, and β is an arbitrary shape factor. The local value of **u** or γ $(e.g., \phi)$ is then calculated as

$$\phi = \chi\phi_{computed} + (1 - \chi)\phi_{target}$$

where ϕ_target is the analytical solution in the inlet relaxation zone and 0 in the outlet zone, and $\phi\_computed$ is the numerical solution.

In addition to reducing reflection coefficients within the computational domain, reflection zones can also attenuate unwanted nonlinear phenomenon at the wave-maker inlet like parasitic waves. The primary drawback of the method is computational cost. In order to work effectively, relaxation zones have to be on the order of one wavelength, increasing the computational domain by two wavelengths in total. Some methods have been developed to shorten the length of the zones necessary to achieve sufficient reflection attenuation, however some involve using a larger mesh which can trigger instability in the volume-fraction equation if a robust advection scheme is not chosen.

IMPLEMENTATION

The following 2-dimensional numerical experiment in OpenFOAM is based off physical experiments conducted at MIT's Nepf Lab as described in (Zhang, Lin, & Nepf, 2014). Although the mathematical model explored in the paper varies from that employed in this project, the accompanying experiment makes for a simple test case. Figure 2. Diagram detailing the computational domain for the present test case, based of physical experiments conducted in the Nepf Lab and described in (Zhang et al. 2014)illustrates the computational domain as it relates to the physical experiment. Note the computational domain is 24 m long as is the flume at the Nepf Lab, both which include the numerical and physical versions of a wave-maker and a sponge layer at the boundaries, respectively. Simplifying slightly, I chose to model my porous media zone at 0.3 m and only ran the simulation at a water depth of 0.4 m.

Grid resolution was set at Δx_1 of 0.05m and a Δx_2 of 0.01. In the '*porousWaveFoam*' solver, the Courant Number is checked at every time step and Δt adjusted accordingly to stay within a defined threshold value, in this case, below 0.25. Although the algorithm is run immediately, the change is dampened over multiple time steps to limit spurious oscillations (Jacobsen, Fuhrman, & Fredsøe, 2012).

I ran the simulation with and without the porous zone at the initial mesh size, then compared this to a second simulation at a much finer grid size, decreasing both Δx_1 and Δx_2 by a factor of 2. This is assumed the "exact" solution and values are compared to verify convergence.

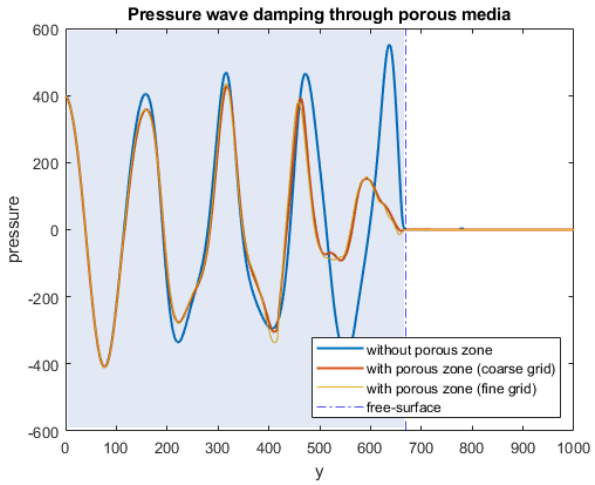

Figure 3.Illustrates the effect of the porous media zone on the vertical distribution of the pressure wave.

Plots of the solutions to the volume-fraction equation (*'alpha.water'*), the non-hydrostatic pressure field, and the u magnitude for the most coarse grid case at t = 20s are illustrated in Figure 4. Plots of the a) non-hydrostatic pressure field, b) volume fraction equation, and c) velocity magnitude at t = 20s for the coarse grid simulation, while animations of those same solutions are linked in the appendix. The effect of the vegetation patch on the incoming waves is very apparent visually, however more post-processing analysis is required before I'm able to quantify the resulting C_D. As a preliminary step, Figure 3.Illustrates the effect of the porous media zone on the vertical distribution of the pressure wave. plots the

vertical pressure distribution at the centerline of the computational domain for both the porous and non-porous media case at the coarse mesh size, as well as the porous case at the fine mesh size.

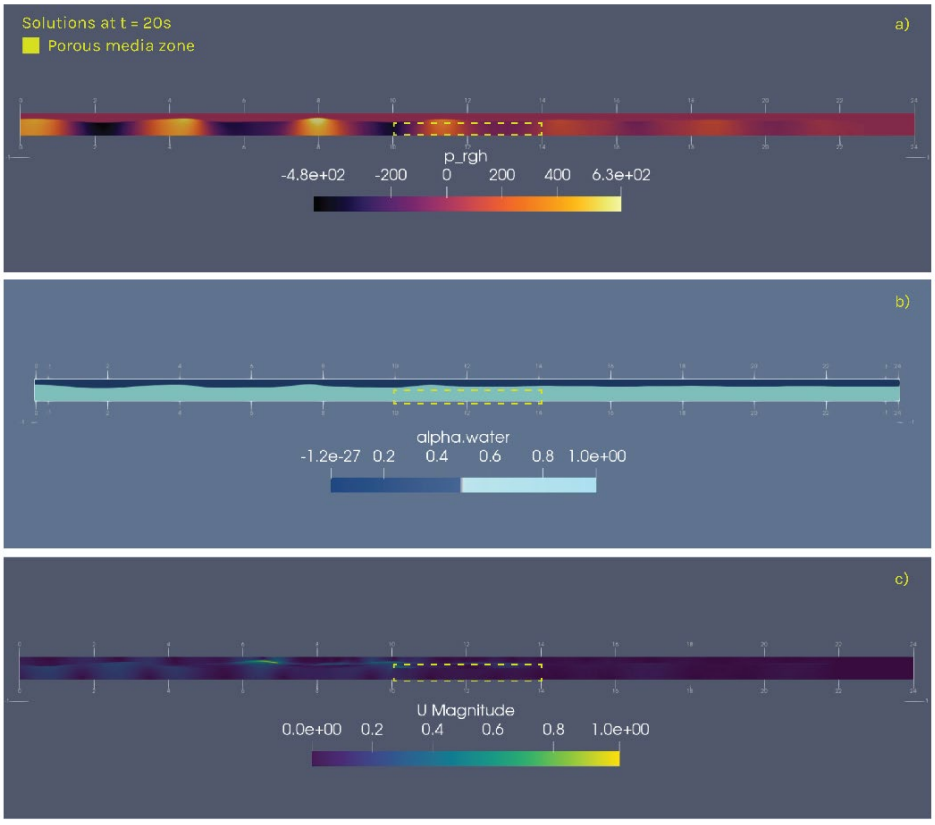

Figure 4. Plots of the a) non-hydrostatic pressure field, b) volume fraction equation, and c) velocity magnitude at t = 20s for the coarse grid simulation

NEXT STEPS

Although the model seems promising, more numerical validation needs to be done to determine accuracy and error. I hope to obtain the raw data from the experiment described in (Zhang, Lin, & Nepf, 2014) so that I can determine the numerically given drag coefficient and compare it against experimental values. I also want to manually calculate the wave reflection coefficient and check whether my relaxation zones are appropriately sized. I would also want to explore different water depths and porosity values for the vegetated field.

Another interesting line of questioning concerns turbulence closure. As mentioned previously, this model ignores the effects of eddy viscosity, aggregating the turbulent fluctuation term into the overall resistance term F_i much like the model described by (Jensen, Jacobsen, & Christensen, 2014). In (Hadadpour, Paul, & Oumeraci, 2019), a separate turbulence closure model is incorporated, namely $\kappa - \omega - SST$. It could be interesting to explore the effects of different turbulence models on initial wave parameters that lead to breaking.

CONCLUSIONS

CFD is cool! Thanks for an enjoyable semester.

APPENDIX

wavePorousVeg - YouTube

wavePorousVegPressure - YouTube

wavePorousVegU - YouTube

REFERENCES

Augustin, L., Irish, J., & and Lynett, P. (2009). Laboratory and numerical studies of wave damping by emergent and near-emergent wetland vegetation. *Coastal Engineering, 56(3)*, 332-340.

Barbier, E., Hacker, S., Kennedy, C., Koch, E., Stier, A., & Silliman, B. (2011). The value of estuarine and coastal ecosystem services. *Ecological Monographs, 81*, 169-193.

Ferziger, J. H., Perić, M., & & Street, R. L. (2002). *Computational methods for fluid dynamics.* Berlin: Springer.

Hadadpour, S., Paul, M., & Oumeraci, H. (2019). Numerical investigation of wave attentuation by rigid vegetation based on a porous media approach. *Journal of Coastal Research, 92(SI)*, 92-100.

Hu, K., Chen, Q., & Wang, H. (2015). A numerical study of vegetation impact on reducing storm surge by wetlands in a semi-enclosed estuary. *Coastal Engineering, 95*, 66-76.

Jacobsen, N. G., Fuhrman, D. R., & Fredsøe, J. (2012). A wave generation toolbox for the open-source CFD library: OpenFoam (R). *International Journal for Numerical Methods in Fluids, 9*, 1073-1088.

Jensen, B., Jacobsen, N. G., & Christensen, E. D. (2014). Investigation on the porous media equations and resistance coefficients for coastal structures. *Coastal Engineering, 84*, 56-72.

Li, C., & and Yan, K. (2007). Numerical investigation of wave-current-vegetation interaction. *Journal of Hydraulic Engineering, 133(7)*, 794-803.

Mendez, F., & Losada, I. (2004). An empirical model to estimate the propagation of random breaking and nonbreaking waves over vegetation fields. *Coastal Engineering, 51(2)*, 103-118.

Moosavi, S. (2017). Ecological Coastal Protection: Pathways to Living Shorelines. *Procedia Engineering, 196*, 930-938.

Munsch, S. H., Cordell, J. R., Toft, J. D., & Morgan, E. E. (2014). Effects of seawalls and piers on fish assemblages and juvenile salmon feeding behavior. *North American Journal of Fisheries Management 34(4)*, 814-827.

Rocco, G., Coppola, G., & & De Luca, L. (2010). The VOF method applied to the numerical simulation of a 2D liquid jet under gravity. *WIT Trans. Eng. Sci, 69*, 207-217.

Sutherland, J., Obhrai, C., Whitehouse, R., & Pearce, A. (2007). Laboratory tests of scour at seawall. *ICSE 2006 (3rd International Conference on Scour and Erosion)*, (pp. 3-5). Gouda, The Netherlands.

Torio, D. D., & Chmura, G. L. (2013). Assessing Coastal Squeeze of Tidal Wetlands. *Journal of Coastal Research, 29(5)*, 1049-1061.

Van Gent, M. R. (1995). Porous flow thorugh rubble-mound material. *Journal of waterway, port, coastal, and ocean engineering, 121(3)*, 176-181.

Wu, W., & Marsooli, R. (2012). A depth-averaged 2D shallow water model for breaking and non-breaking long waves affected by rigid

vegetation. *Journal of Hydraulic Research, 50(6)*, 558-575.

Yamasaki, T. N., de Lima, P. H., Silva, D. F., Cristiane, G. D., Janzen, J. G., & Nepf, H. M. (2019). From patch to channel scale: The evolution of emergent vegetation in a channel. *Advances in Water Resources, 129*, 131-145.

Zhang, X., Lin, P., & Nepf, H. (2014). A simple-wave damping model for flexible marsh plants. *Limnol. Oceanogr. 9999*, 1-15.

Zinke, P. (2012). Application of porous media approach for vegetation flow resistance. *Proceedings of River Flow 2012*, (pp. 301-310). San Jose, Costa Rica.

Special thanks to Wael Hajj Ali (: